

## Article

# Spin Label Study of the Orientational Preferences of Lysozyme in a Bioinspired Silica Composite

Francesco Bruno <sup>1,2,3</sup> , Lucia Gigli <sup>4</sup> and Enrico Ravera <sup>1,2,3,\*</sup> <sup>1</sup> Department of Chemistry “Ugo Schiff”, University of Florence, 50019 Sesto Fiorentino, Italy<sup>2</sup> Magnetic Resonance Center (CERM), University of Florence, 50019 Sesto Fiorentino, Italy<sup>3</sup> Consorzio Interuniversitario Risonanze Magnetiche di Metallo Proteine, 50019 Sesto Fiorentino, Italy<sup>4</sup> Computational Systems Chemistry, School of Chemistry, University of Southampton, Southampton SO17 1BJ, UK

\* Correspondence: ravera@cerm.unifi.it

**Abstract:** Polycationic polypeptides prompt the polycondensation of inorganic oxides, most notably of silica. Hen egg-white lysozyme is a small polycationic protein that is quite conveniently used to this end. The fate of the protein after the completion of the polycondensation reaction is still a matter of debate. We have recently proven that lysozyme strongly interacts with silica. In this study, we use spin-label-based EPR spectroscopy to investigate whether the protein shows an orientational preference with respect to the silica surface within the composite. We find that a large share of the protein behaves as when it is adsorbed on pre-formed silica, albeit with a more marked preference for orientations that point the patches with higher surface charge density toward the material. In addition, a part of the protein shows a less-defined behavior. With this study, we provide additional information on the nature of the protein-material interactions in this class of bioinspired solids.

**Keywords:** biosilica; polycondensation; polycationic proteins



**Citation:** Bruno, F.; Gigli, L.; Ravera, E. Spin Label Study of the Orientational Preferences of Lysozyme in a Bioinspired Silica Composite. *J. Compos. Sci.* **2023**, *7*, 188. <https://doi.org/10.3390/jcs7050188>

Academic Editor: Francesco Tornabene

Received: 13 March 2023

Revised: 18 April 2023

Accepted: 4 May 2023

Published: 6 May 2023



**Copyright:** © 2023 by the authors. Licensee MDPI, Basel, Switzerland. This article is an open access article distributed under the terms and conditions of the Creative Commons Attribution (CC BY) license (<https://creativecommons.org/licenses/by/4.0/>).

## 1. Introduction

The production of silica nanoparticles is highly relevant in contemporary industrial inorganic chemistry, and other types of metal oxide nanocomposites are also being explored in fundamental research for biological and catalytic applications. However, the standard synthetic routes to the production of inorganic oxides (e.g. the Stöber process for silica) are inherently poorly sustainable and have a large environmental footprint [1] because they involve the use of noxious or non-sustainable chemicals such as petrochemical surfactants, alcohols, and strong acids and bases, as well as the need for heat treatment to obtain condensed silica networks.

A major breakthrough with enormous industrial potential and the opportunity of decreasing the environmental footprint of the formation of inorganic oxides is provided by bioinspired mineralization approaches [2]. As the name implies, these approaches are inspired by the natural biomineralization mechanisms, which occur under conditions that are inherently compatible with life [3–5]. One remarkable example is indeed silica, which is chemically obtained by either acid or basic catalysis, forming a sol that is strengthened the farthest from pH = 7. The sol/gel is subsequently heated above 800 °C to form a glass [6]. By contrast, several organisms can form highly condensed silica deposits at room temperature and neutral pH by the catalytic effect of silicateins [7], which promote the formation of *spiculae* in sponges, or silaffins [8], which promote the formation of diatoms' exoskeleta. Notably, these proteins and peptides induce the formation of silica in vitro and also promote the formation of deposits of other inorganic oxides, for example, titania [9,10]. In these composites, the interactions occurring on the molecular scale affect the stability and the reactivity of the material. Thus, understanding the interplay between the protein and the material component is expected to be a breakthrough in nano-biotechnologies

because it can lead to “quality by design” strategies for the development of new catalysts for industrial applications and for biomedical devices.

Under the assumption that it is the electrostatic effect of polycationic biological macromolecules that drives the silica patterning [11,12], Luckarift et al. selected lysozyme, a 14 kDa polycationic protein ( $pI = 10.7$ ), as a catalyst, and demonstrated that it could as well promote the polycondensation of silica from solutions of tetraoxosilicic(IV) acid and titania from titanium(IV)-bis ammonium lactate [13]. A synthetic strategy based on the use of lysozyme is convenient even with respect to the use of polycationic peptides because lysozyme is relatively inexpensive and can be even recovered from food processing wastes [14]. Furthermore, it has been proven that by adapting the synthesis conditions, the morphology of the silica-lysozyme composites can be controlled [15]. We have recently focused our attention on the mechanistic and structural aspects of the preparation of these composites, and we have demonstrated that a hydrolyzed species of the titanium(IV) precursor is found interacting with an area of denser positive charge at the protein surface [16]. What happens to the protein after templating the condensed silica network has been a subject of debate. The Luckarift et al. original paper reports that the protein is not removed upon repeated washing cycles and that it retains its antimicrobial activity. It is also reported that the protein accounts for a large share of the dry mass of the material (50–62% [13,17]). A recent study based on the analysis of the SAXS profiles recorded in both adsorption and co-precipitation experiments concluded that the protein is not trapped inside the silica but is rather partially unfolded and adsorbed [18]. The residual antimicrobial activity would then be due to the unfolded protein only [19]. The same authors used time-resolved SAXS to characterize the early phases of the polymerization and concluded that the protein unfolds significantly and only partly regains its structure in the final composite [20]. However, we and others have found by  $^{13}\text{C}$  solid-state magic angle spinning NMR, which bears intrinsically higher resolution information on the state of the protein component, that the protein fold is not significantly altered in the composite [21–23]. We then tested the behavior of the composite with respect to washing, and we found, in line with Luckarift et al., that the protein is not washed away from the material using water. We have also found that only a part (ca. 20%) is washed out with a high concentration of sodium chloride and that only denaturation with guanidinium hydrochloride (equivalently with urea) and reduction with dithiothreitol can fully release the protein from the material. Collectively, these results suggest that electrostatic interactions only account for 20% of the protein being in contact with the outer surface of the material, and most of the protein (80%) is somehow occluded within the composite. This is compatible with the results obtained by high-temperature treatment—hence the removal of lysozyme by carbonization—that are reported in [13] and in [17]. In [13], the electron microscopy characterization after the carbonization of lysozyme shows carbon spots on the outer surface. At the same time, the nitrogen adsorption/desorption isotherms reported in [17] can be interpreted as the removal of lysozyme by carbonization is leaving behind a large-pore mesoporous structure. In turn, this implies that the removal of the protein creates cavities or, from the protein standpoint, that the protein is confined within pores or other networks composed of smaller silica particles (microscopy measurements show particles with radii of the order of 200–300 nm [13,17], whereas the SAXS measurements indicate that the radii of the silica primary units are of the order of 4 nm [17,23]). Thus, the interaction between the protein and the material concerns both the outer surface of the material but also the surface of the inner structural components of silica. From the analysis of  $\{^1\text{H}\}$ - $^{13}\text{C}$  HETCOR and  $\{^1\text{H}\}$ - $^{29}\text{Si}$  HETCOR [24–26] spectra acquired on the composite [23,27], we could prove that lysozyme remains in tight contact with surface  $^{29}\text{Si}$  species of condensed silica, but it is not covalently bound, as opposed with what is observed in the case of the polycationic peptide PL12 [28]. However, the molecular details of this interaction remain elusive.

In a recent study, Antonov et al. [29] used Electron Paramagnetic Resonance (EPR) spectroscopy, spin-labeling lysozyme with a nitroxide moiety at residue H15, to examine the orientational preferences of a lysozyme physisorbed on or cross-linked to a series of

pre-formed porous oxide carriers, including silica. Spin labels (or, now less commonly, spin probes) are stable radicals, usually nitroxides, that are attached to proteins to obtain information about the hydration and motion of the protein [30]. Nitroxide radicals are particularly attractive because of their intrinsic asymmetry, which gives rise to an asymmetric pattern when the reorientation is impeded, which makes it easy to discriminate between different degrees of mobility (see, for instance, [31]). The other appealing feature of nitroxides is that when one particular nitroxide is selected (e.g., a TEMPO derivative) and conditions like solvent polarity are not changed [32], the spin Hamiltonian parameters  $A$  and  $g$  are relatively stable. Spin-labeling with nitroxide thus allows for easy monitoring of the behavior of the same chemical system (in this case, lysozyme spin-labeled at the H15 position with iodoacetamido-TEMPO using the same spin Hamiltonian parameters across a series of different conditions).

In [29], the authors distinguished two types of immobilization modes: Type I, in which the spin label has similar mobility with respect to the free protein in solution, hence with H15 pointing toward the solution, and Type II, in which the spin label has sizably reduced mobility, hence with H15 pointing toward the surface. The different relative amount of Type I and Type II adsorption reflects the positioning of H15: it is located within a patch of high positive potential (Figure 1), which can prompt adsorption toward negatively charged silica [29], and therefore it is expected that an increase of Type II content reflects a stronger electrostatic interaction.

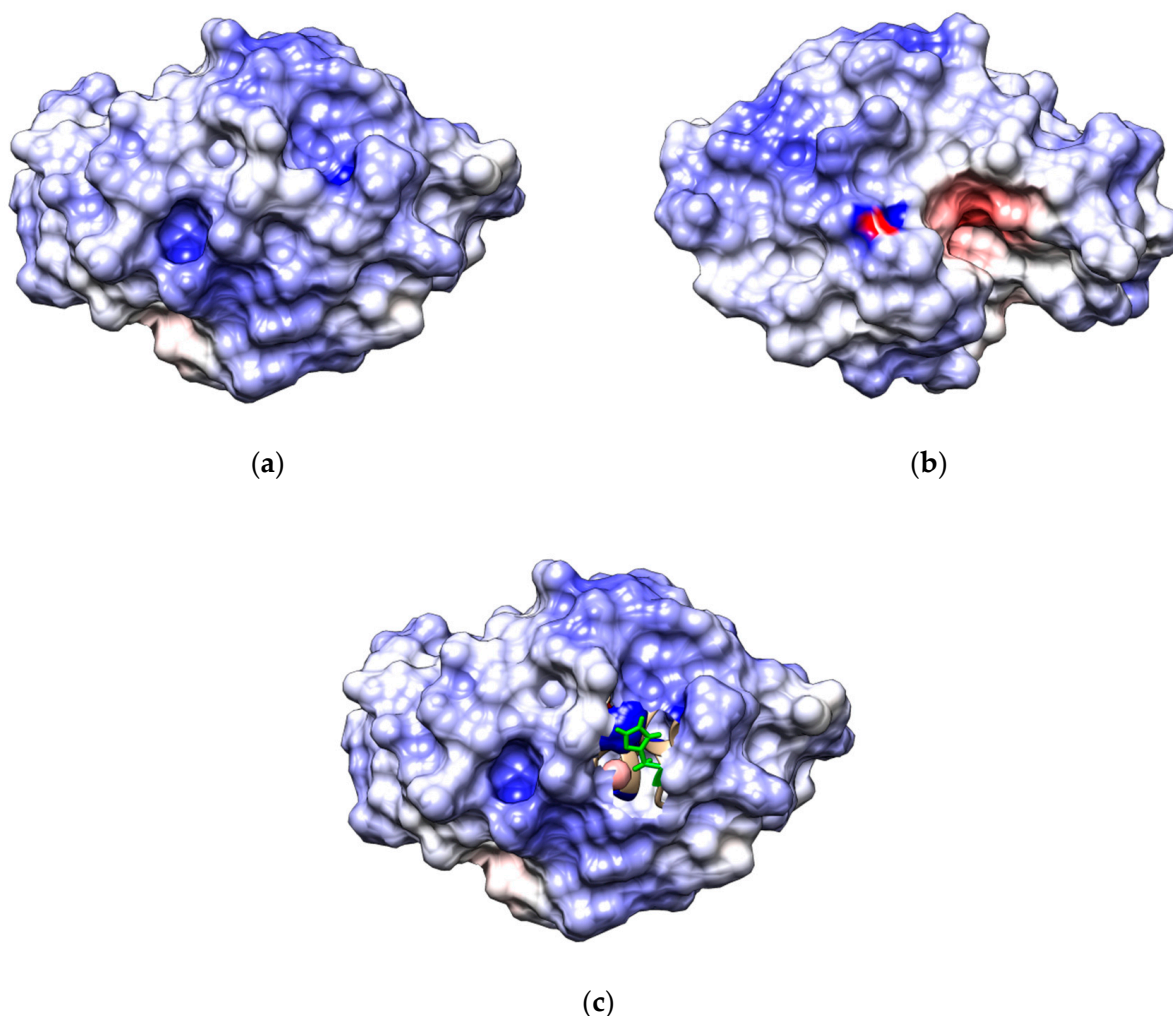


**Figure 1.** Electrostatic potential of lysozyme mapped on its solvent accessible surface (color code is blue-positive (256 mV)/red-negative (−256 mV)). Panels (a,b) are 180° rotated along the page axis. Panel (c) shows the same orientation as (a), revealing H15 in green.

In the present manuscript, we apply the same experimental strategy to understand whether lysozyme shows any orientational preference in presenting its surface to the silica surface in the bioinspired silica-lysozyme composite prepared according to Luckarift et al. [13], where the silica is grown in the presence of the protein rather than mixed a posteriori with pre-formed materials.

## 2. Materials and Methods

Lysozyme was obtained from Sigma (Kawasaki, Japan) and used without further purification. The reaction for spin-labeling H15 was performed using 4-(2-iodoacetamido)-2,2,6,6-tetramethylpiperidine 1-oxyl (4-(2-iodoacetamido)-TEMPO), also from Sigma, under the conditions described in [29,32,33], and the spin-labeled lysozyme was separated from the reaction mixture using a desalting column. Then, the protein was used to prepare the silica composite according to [13]: lysozyme solution at 10 mg/mL concentration was mixed with a solution of freshly prepared silicic acid (obtained by hydrolysis of TMOS by HCl at 1 mmol·dm<sup>-3</sup>) buffered at pH 8 using TRIS. No crosslinking agents have been added. After 15 min, the reaction mixture is centrifuged at 10,000× g for 3 min and washed three times with water as described in [23].

EPR spectra were acquired at X-band (9.77 GHz) on a Bruker ELEXSYS spectrometer equipped with a standard Bruker ST4102 cavity. Four scans were taken for each sample under ambient conditions. MW power was set to 5 mW; no evidence of saturation was observed. Modulation field was 1 G at 30 kHz, which should cause no significant linewidth alteration in a spectrum in which the narrowest feature is of the order of 2 G [34,35].

The EPR spectra were calculated in the slow-motion regime using the chili function from Easyspin [35]. The model-free calculation of **g** and **A** parameters modulated by quasibrations was implemented as described in [36,37]. The hyperfine interaction tensor **A** is calculated as

$$\begin{aligned}\langle A_x \rangle &= A_x + \frac{1}{2}(A_z - A_x)(1 - P_y) + \frac{1}{2}(A_y - A_x)(1 - P_z) \\ \langle A_y \rangle &= A_y + \frac{1}{2}(A_z - A_y)(1 - P_x) + \frac{1}{2}(A_x - A_y)(1 - P_z) \\ \langle A_z \rangle &= A_z + \frac{1}{2}(A_x - A_z)(1 - P_y) + \frac{1}{2}(A_y - A_z)(1 - P_x)\end{aligned}$$

where  $P_x = \frac{\sin L_x \cos L_x}{L_x}$ ,  $P_y = \frac{\sin L_y \cos L_y}{L_y}$ , and  $P_z = \frac{\sin L_z \cos L_z}{L_z}$ , and  $L_x$ ,  $L_y$ , and  $L_z$  are half-amplitudes of the quasibrillation motion around the  $x$ ,  $y$ , and  $z$  magnetic axes, respectively. The **g** tensor is calculated analogously. When fitted, the quasibrillation amplitudes can correlate with the reorientation diffusion tensor components [37]. The MATLAB function for the averaging is given in the supporting information.

Literature values for **g** and **A** of the TEMPO moiety are given in Table 1 [29].

**Table 1.** EPR spin Hamiltonian parameters for the TEMPO moiety taken from ref. [29].

Parameter	xx	yy	zz	Isotropic
<b>g</b>	2.0088	2.0064	2.0024	2.0059
<b>A</b> /MHz	18.5	18.2	106	47.5

The electrostatic potential of lysozyme (cpr. Figure 1 above) has been calculated using the APBS web server [38] on the 6F1O structure [39], which has been proven to be the structure closest to the free protein in solution [40].

### 3. Results and Discussion

The EPR spectrum of H15-spin-labeled lysozyme in the composite is shown in Figure 2.

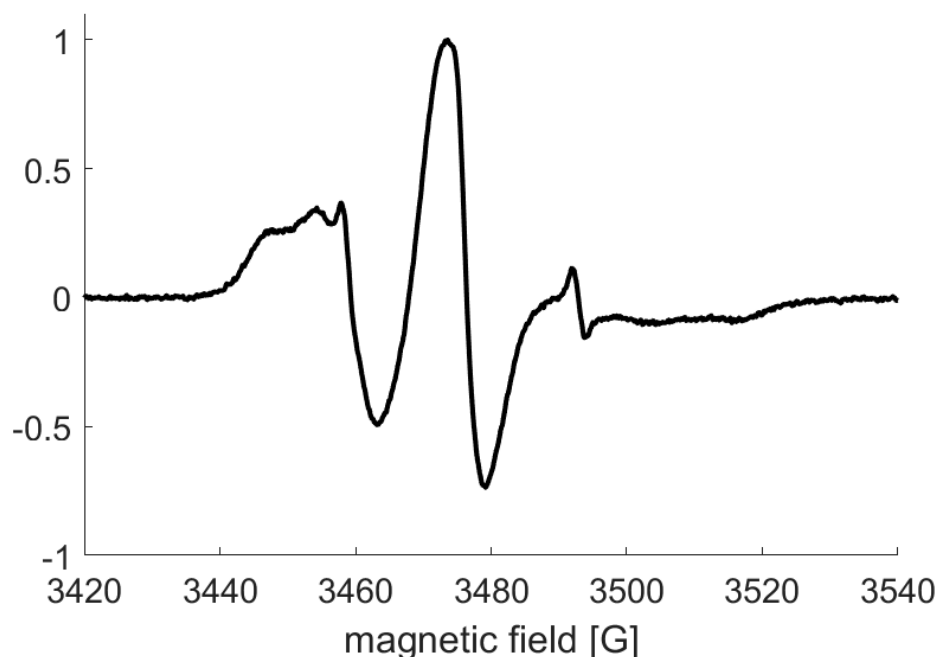


**Figure 2.** Experimental spectrum of spin-labeled lysozyme in the composite.

It is apparent that the spectrum shows the presence of multiple species with different degrees of immobilization [41]. The two broad high-field features (3517 G and 3505 G) can be attributed to two slowly reorienting species—respectively—one species where the spin label motion is suppressed and one where the protein reorientation has been slowed down significantly, but the radical is still able to reorient. This situation is clearly reminiscent of the results by Antonov et al. [29], mentioned above: the species that reorients slowly but in which the spin label has a reorientational freedom comparable to the free protein can be related to Type I adsorption, whereas the species where the radical reorientation is drastically reduced can be related to Type II adsorption. We have thus attempted to reproduce the spectra using the same species used by Antonov et al. [29]. The sharpest features correspond to the free radicals and free proteins and account for a minor fraction of the sample (below 1%, *vide infra*). Using the spin Hamiltonian parameters from [29] and adjusting the line widths of the adsorbed species and the relative weights of the species, the fit is shown in Figure 3, and Supplementary Figure S1 is obtained. Fitting parameters are given in Table 2.

The fit can be marginally improved by allowing the spin Hamiltonian parameters to vary within a reasonable range (the sum of the squared normalized residuals is 1.91, Figure S2 and Table S1). In any case, the residuals of these fits show a clear systematic deviation; hence the considered forms cannot account for the appearance of the spectrum. Some important indications can already be gathered. For instance, it is apparent that the Type II adsorption mode is favored over Type I, more than in the cases presented by Antonov et al. [29]. This behavior can be qualitatively explained on the basis of the electrostatic potential of the lysozyme (cpr. Figure 1): it should be bore in mind that H15 is located within a positively charged patch on the protein surface, which can prompt adsorption toward negatively-charged silica [29]. Unsurprisingly, this is also the location at which a hydrolyzed titanium(IV) species has been previously observed by us in crystals soaked with a titanium oxide precursor [16]. This suggests that the electrostatic interactions, although not dominant for retaining most of the protein within the composite [23], are still relevant to induce an orientational preference of the protein with respect to the silica surface.

This is also consistent with our previous observations on ubiquitin that suggest that the bioinspired silica has a high negative surface charge, comparable to MCM silica [42].

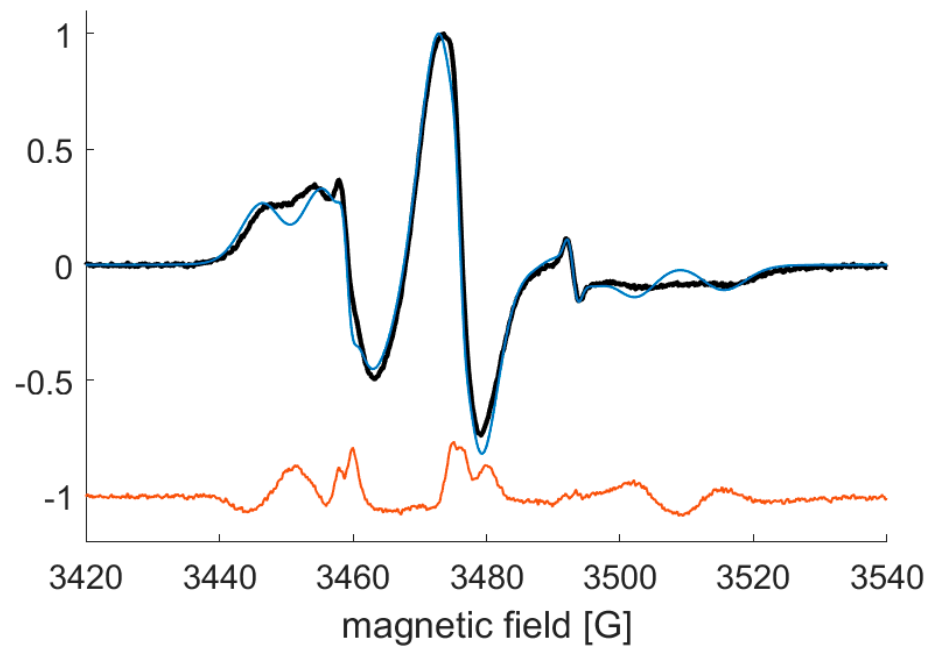


**Figure 3.** Experimental EPR spectrum of spin–labeled lysozyme in the composite (black), and result of the 4-components simulation using the parameters from Table 2 (blue). The residuals of the fit are shown in orange. The sum of the squared normalized residuals is 2.52.

**Table 2.** Components used for the fit reported in Figure 2 [29]. lwpp indicates a gaussian broadening.

Component	Rotational Diffusion Coefficients ( $\times 10^6 \text{ s}^{-1}$ )	lwpp (G)	$L_x$ ( $^\circ$ )	$L_y$ ( $^\circ$ )	$L_z$ ( $^\circ$ )	Weight (%)
Free radical	$4.0 \times 10^3$	1.5	0	0	0	0.54
Free protein	22, 28, 12	1.5	62	34	45	0.36
Type I	2.9	5.1	62	34	45	30.3
Type II	2.9	6.0	20	20	20	68.8

We have also performed a fit with the addition of a component that has less restricted mobility with respect to Type II but has smaller libration amplitudes with respect to Type I, which we will refer to as Type Ir (Table 3). We hypothesize that this species has H15 pointing toward the solvent but being restricted by interprotein crowding effects or by the occluding effect of a pore/cage made of several silica primary unit, consistent with our previous findings. This component improves the quality of the fit (sum of squared residuals 1.65), but the systematic deviation of the residuals remains (Figures 4 and S3).

**Table 3.** Parameters of the fit of the EPR spectrum as shown in Figure 4.

Component	Rotational Diffusion Coefficients ( $\times 10^6 \text{ s}^{-1}$ )	lwpp (G)	$L_x$ ( $^\circ$ )	$L_y$ ( $^\circ$ )	$L_z$ ( $^\circ$ )	Weight (%)
Free radical	$4.0 \times 10^3$	1.5	0	0	0	0.41
Free protein	22, 28, 12	1.5	62	34	45	0.13
Type I	2.9	4.7	62	34	45	6.31
Type Ir	2.9	4.7	57	22	20	33.4
Type II	2.9	5.8	20	20	20	58.6

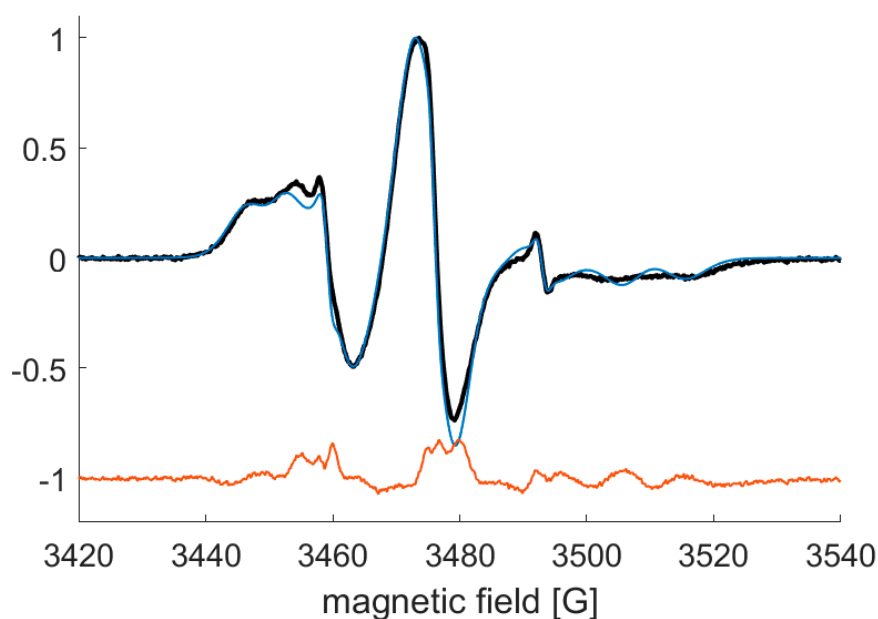


**Figure 4.** Experimental EPR spectrum of spin-labeled lysozyme in the composite (black) and result of the 5-components simulation using the parameters from Table 3 (blue). The residuals of the fit are shown in orange. The sum of the squared normalized residuals is 1.65.

The simulation shown in Figures 4 and S2 suggests that other species with even more reduced librational freedom exist in this sample. However, the information content of the data is not sufficient to determine the weight of an additional species, and even if it did, no additional chemical insight could be garnered at this level of resolution.

#### 4. Conclusions

The use of lysozyme as a templating molecule has been proposed for a more energy-efficient production of silica particles more than a decade ago. However, little is known about the architecture of the resulting composite and the fate of the protein as a result of the entrapment. In previous works, we have proven that the structure of lysozyme is preserved, and the NMR results implied that the protein strongly interacts with the silica either via direct hydrogen bonding or through intervening water molecules. Our previous results also show that purely electrostatic interaction is responsible for only 20% of the protein being retained on the most accessible surfaces of the silica particles, whereas 80% of the protein results sterically trapped within a network composed of primary silica units that are of the order of nanometers. Even if the electrostatic component of the interaction plays a supporting role in retaining the protein within the material, the results we present in this manuscript suggest that electrostatics play a significant role in determining the orientation of the protein relative to the silica surface, with a preference for adsorption at the most positively-charged surface. Intriguingly, electrostatics appear to play a more significant role than in physisorbed samples from previous studies. Incidentally, since Type II adsorption is favored, a larger share of the protein presents the active site toward the solvent. The features of the EPR spectra suggest that the motion of lysozyme in the composite has a more diverse spectrum of restriction levels than lysozyme physisorbed on pre-prepared silica. We can speculate that this can be due to the crowding imposed by the relatively high concentration of lysozyme in the composite and by the occluding steric effect of the inorganic matrix.

**Supplementary Materials:** The following supporting information can be downloaded at: <https://www.mdpi.com/article/10.3390/jcs7050188/s1>, Figure S1: Experimental EPR spectrum of spin-labelled lysozyme in the composite (black), and individual traces of the 4 components simulation shown in Figure 2; Figure S2: Experimental EPR spectrum of spin-labelled lysozyme in the composite (black), and individual traces of the 4 components simulation (Table S1). Squared sum of the residuals 1.91; Table S1: Components used for the fit reported in Figure S2.; Figure S3: Experimental EPR spectrum of spin-labelled lysozyme in the composite (black), and individual traces of the 5 components simulation shown in Figure 2; EPR data; MATLAB function for calculating quasibration averaging.

**Author Contributions:** Conceptualization, F.B., L.G. and E.R.; Sample preparation, F.B. and L.G.; EPR spectroscopy, L.G. and E.R.; software, E.R.; writing, F.B., L.G. and E.R.; supervision, E.R.; funding acquisition, E.R. All authors have read and agreed to the published version of the manuscript.

**Funding:** This work has been supported by the project “Potentiating the Italian Capacity for Structural Biology Services in Instruct-ERIC—ITACA.SB” (Project no. IR0000009) within the call MUR 3264/2021 PNRR M4/C2/L3.1.1, funded by the European Union NextGenerationEU, by the Italian Ministero dell’Università e della Ricerca through the “Progetto Dipartimenti di Eccellenza 2023–2027 (DICUS2.0)” to the Department of Chemistry “Ugo Schiff” of the University of Florence. F.B. and E.R. acknowledge the Italian Ministry of Education, University and Research (MIUR), and European Social Fund (ESF) for the PON R&I 2014–2020 program, actions IV.5 “Doctorates and research contracts on Green topics”. The authors acknowledge the support and the use of resources of Instruct-ERIC, a landmark ESFRI project, and specifically the CERM/CIRMMMP Italy centre.

**Data Availability Statement:** The EPR data and the matlab function to calculate averaging by quasibrations are provided as supporting information.

**Conflicts of Interest:** The authors declare no conflict of interest.

## References

1. Curley, R.; Holmes, J.D.; Flynn, E.J. Can Sustainable, Monodisperse, Spherical Silica Be Produced from Biomolecules? A Review. *Appl. Nanosci.* **2021**, *11*, 1777–1804. [[CrossRef](#)]
2. Vrieling, E.G.; Beelen, T.P.M.; van Santen, R.A.; Gieskes, W.W.C. Diatom Silicon Biomineralization as an Inspirational Source of New Approaches to Silica Production. *J. Biotechnol.* **1999**, *70*, 39–51. [[CrossRef](#)]
3. Wang, X.; Schröder, H.C.; Müller, W.E.G. Enzyme-Based Biosilica and Biocalcite: Biomaterials for the Future in Regenerative Medicine. *Trends Biotechnol.* **2014**, *32*, 441–447. [[CrossRef](#)] [[PubMed](#)]
4. Kim, D.W.; Lee, O.J.; Kim, S.-W.; Ki, C.S.; Chao, J.R.; Yoo, H.; Yoon, S.-I.; Lee, J.E.; Park, Y.R.; Kweon, H.; et al. Novel Fabrication of Fluorescent Silk Utilized in Biotechnological and Medical Applications. *Biomaterials* **2015**, *70*, 48–56. [[CrossRef](#)] [[PubMed](#)]
5. Rodriguez-Maciá, P.; Dutta, A.; Lubitz, W.; Shaw, W.J.; Rüdiger, O. Direct Comparison of the Performance of a Bio-Inspired Synthetic Nickel Catalyst and a [NiFe]-Hydrogenase, Both Covalently Attached to Electrodes. *Angew. Chem. Int. Ed. Engl.* **2015**, *54*, 12303–12307. [[CrossRef](#)]
6. Hench, L.L.; West, J.K. The Sol-Gel Process. *Chem. Rev.* **1990**, *90*, 33–72. [[CrossRef](#)]
7. Müller, W.E.G.; Schröder, H.C.; Burghard, Z.; Pisignano, D.; Wang, X. Silicateins—A Novel Paradigm in Bioinorganic Chemistry: Enzymatic Synthesis of Inorganic Polymeric Silica. *Chem. Eur. J.* **2013**, *19*, 5790–5804. [[CrossRef](#)]
8. Kröger, N.; Deutzmann, R.; Sumper, M. Silica-Precipitating Peptides from Diatoms the chemical structure of silaffin-1A from *cylindrotheca fusiformis*. *J. Biol. Chem.* **2001**, *276*, 26066–26070. [[CrossRef](#)]
9. Wiens, M.; Link, T.; Elkhooly, T.A.; Isbert, S.; Müller, W.E.G. Formation of a Micropatterned Titania Photocatalyst by Microcontact Printed Silicatein on Gold Surfaces. *Chem. Commun.* **2012**, *48*, 11331. [[CrossRef](#)]
10. Sewell, S.L.; Wright, D.W. Biomimetic Synthesis of Titanium Dioxide Utilizing the R5 Peptide Derived from *Cylindrotheca Fusiformis*. *Chem. Mater.* **2006**, *18*, 3108–3113. [[CrossRef](#)]
11. Kröger, N.; Deutzmann, R.; Sumper, M. Polycationic Peptides from Diatom Biosilica That Direct Silica Nanosphere Formation. *Science* **1999**, *286*, 1129–1132. [[CrossRef](#)]
12. Coradin, T.; Durupthy, O.; Livage, J. Interactions of Amino-Containing Peptides with Sodium Silicate and Colloidal Silica: A Biomimetic Approach of Silicification. *Langmuir* **2002**, *18*, 2331–2336. [[CrossRef](#)]
13. Luckarift, H.R.; Dickerson, M.B.; Sandhage, K.H.; Spain, J.C. Rapid, Room-Temperature Synthesis of Antibacterial Bionanocomposites of Lysozyme with Amorphous Silica or Titania. *Small* **2006**, *2*, 640–643. [[CrossRef](#)]
14. Cheng, C.-Y.; Wang, M.-Y.; Suen, S.-Y. Eco-Friendly Polylactic Acid/Rice Husk Ash Mixed Matrix Membrane for Efficient Purification of Lysozyme from Chicken Egg White. *J. Taiwan Inst. Chem. Eng.* **2020**, *111*, 11–23. [[CrossRef](#)]
15. Garakani, T.M.; Wang, H.; Krappitz, T.; Liebeck, B.M.; van Rijn, P.; Böker, A. Lysozyme–Silica Hybrid Materials: From Nanoparticles to Capsules and Double Emulsion Mineral Capsules. *Chem. Commun.* **2012**, *48*, 10210–10212. [[CrossRef](#)]

16. Gigli, L.; Ravera, E.; Calderone, V.; Luchinat, C. On the Mechanism of Bioinspired Formation of Inorganic Oxides: Structural Evidence of the Electrostatic Nature of the Interaction between a Mononuclear Inorganic Precursor and Lysozyme. *Biomolecules* **2021**, *11*, 43. [[CrossRef](#)]
17. de Oliveira, L.F.; Gonçalves, K.d.A.; Boreli, F.H.; Kobarg, J.; Cardoso, M.B. Mechanism of Interaction between Colloids and Bacteria as Evidenced by Tailored Silica–Lysozyme Composites. *J. Mater. Chem.* **2012**, *22*, 22851–22858. [[CrossRef](#)]
18. van den Heuvel, D.B.; Stawski, T.M.; Tobler, D.J.; Wirth, R.; Peacock, C.L.; Benning, L.G. Formation of Silica–Lysozyme Composites Through Co-Precipitation and Adsorption. *Front. Mater.* **2018**, *5*, 19. [[CrossRef](#)]
19. Ibrahim, H.R.; Matsuzaki, T.; Aoki, T. Genetic Evidence That Antibacterial Activity of Lysozyme Is Independent of Its Catalytic Function. *FEBS Lett.* **2001**, *506*, 27–32. [[CrossRef](#)]
20. Stawski, T.M.; van den Heuvel, D.B.; Besselink, R.; Tobler, D.J.; Benning, L.G. Mechanism of Silica–Lysozyme Composite Formation Unravelling by in Situ Fast SAXS. *Beilstein J. Nanotechnol.* **2019**, *10*, 182–197. [[CrossRef](#)]
21. Mirau, P.A. Interfacial Structure Determination. In *Bio-Inspired Nanotechnology: From Surface Analysis to Applications*; Knecht, M.R., Walsh, T.R., Eds.; Springer: New York, NY, USA, 2014; pp. 95–125. ISBN 978-1-4614-9446-1.
22. Ravera, E.; Michaelis, V.K.; Ong, T.-C.; Keeler, E.G.; Martelli, T.; Fragai, M.; Griffin, R.G.; Luchinat, C. Biosilica-Entrapped Enzymes Studied by Using Dynamic Nuclear-Polarization-Enhanced High-Field NMR Spectroscopy. *ChemPhysChem* **2015**, *16*, 2751–2754. [[CrossRef](#)] [[PubMed](#)]
23. Bruno, F.; Gigli, L.; Ferraro, G.; Cavallo, A.; Michaelis, V.K.; Goobes, G.; Fratini, E.; Ravera, E. Lysozyme Is Sterically Trapped within the Silica Cage in Bioinspired Silica–Lysozyme Composites: A Multi-Technique Understanding of Elusive Protein–Material Interactions. *Langmuir* **2022**, *38*, 8030–8037. [[CrossRef](#)] [[PubMed](#)]
24. Vinogradov, E.; Madhu, P.K.; Vega, S. High-Resolution Proton Solid-State NMR Spectroscopy by Phase-Modulated Lee–Goldburg Experiment. *Chem. Phys. Lett.* **1999**, *314*, 443–450. [[CrossRef](#)]
25. Vinogradov, E.; Madhu, P.K.; Vega, S. A Bimodal Floquet Analysis of Phase Modulated Lee–Goldburg High Resolution Proton Magic Angle Spinning NMR Experiments. *Chem. Phys. Lett.* **2000**, *329*, 207–214. [[CrossRef](#)]
26. Vinogradov, E.; Madhu, P.K.; Vega, S. Proton Spectroscopy in Solid State Nuclear Magnetic Resonance with Windowed Phase Modulated Lee–Goldburg Decoupling Sequences. *Chem. Phys. Lett.* **2002**, *354*, 193–202. [[CrossRef](#)]
27. Bruno, F.; Francischello, R.; Bellomo, G.; Gigli, L.; Flori, A.; Menichetti, L.; Tenori, L.; Luchinat, C.; Ravera, E. Multivariate Curve Resolution for 2D Solid-State NMR Spectra. *Anal. Chem.* **2020**, *92*, 4451–4458. [[CrossRef](#)]
28. Geiger, Y.; Gottlieb, H.E.; Akbey, Ü.; Oschkinat, H.; Goobes, G. Studying the Conformation of a Silaffin-Derived Pentapeptide Embedded in Bioinspired Silica Using Solution and Dynamic Nuclear Polarization Magic-Angle Spinning NMR. *J. Am. Chem. Soc.* **2016**, *138*, 5561–5567. [[CrossRef](#)]
29. Antonov, D.O.; Chumakova, N.A.; Kovaleva, E.G. Orientation of Spin-Labeled Lysozyme from Chicken Egg White Immobilized on Porous Oxide Carriers. *Appl. Magn. Reson.* **2020**, *51*, 679–690. [[CrossRef](#)]
30. Berliner, L.J. 1-Introduction. In *Spin Labeling*; Berliner, L.J., Ed.; Molecular Biology: An International Series of Monographs and Textbooks; Academic Press: Amsterdam, The Netherlands, 1976; pp. 1–4. ISBN 978-0-12-092350-2.
31. Etienne, E.; Le Breton, N.; Martinho, M.; Mileo, E.; Belle, V. SimLabel: A Graphical User Interface to Simulate Continuous Wave EPR Spectra from Site-Directed Spin Labeling Experiments. *Magn. Reson. Chem.* **2017**, *55*, 714–719. [[CrossRef](#)]
32. Schaich, K.M. Spin Label Study of Water Binding and Protein Mobility in Lysozyme. In *Free Radicals in Food*; ACS Symposium Series; American Chemical Society: Washington, DC, USA, 2002; Volume 807, pp. 98–113. ISBN 978-0-8412-3741-4.
33. Wien, R.W.; Morrisett, J.D.; McConnell, H.M. Spin-Label-Induced Nuclear Relaxation. Distances between Bound Saccharides, Histidine-15, and Tryptophan-123 on Lysozyme in Solution. *Biochemistry* **1972**, *11*, 3707–3716. [[CrossRef](#)]
34. Hyde, J.S.; Pasenkiewicz-Gierula, M.; Jesmanowicz, A.; Antholine, W.E. Pseudo Field Modulation in EPR Spectroscopy. *Appl. Magn. Reson.* **1990**, *1*, 483–496. [[CrossRef](#)]
35. Stoll, S.; Schweiger, A. EasySpin, a Comprehensive Software Package for Spectral Simulation and Analysis in EPR. *J. Magn. Reson.* **2006**, *178*, 42–55. [[CrossRef](#)]
36. Chernova, D.A.; Vorobiev, A.K. Molecular Mobility of Nitroxide Spin Probes in Glassy Polymers. Quasi-Libration Model. *J. Polym. Sci. Part B: Polym. Phys.* **2009**, *47*, 107–120. [[CrossRef](#)]
37. Vorobiev, A.K.; Bogdanov, A.V.; Yankova, T.S.; Chumakova, N.A. Spin Probe Determination of Molecular Orientation Distribution and Rotational Mobility in Liquid Crystals: Model-Free Approach. *J. Phys. Chem. B* **2019**, *123*, 5875–5891. [[CrossRef](#)]
38. Jurrus, E.; Engel, D.; Star, K.; Monson, K.; Brandi, J.; Felberg, L.E.; Brookes, D.H.; Wilson, L.; Chen, J.; Liles, K.; et al. Improvements to the APBS Biomolecular Solvation Software Suite. *Protein Sci.* **2018**, *27*, 112–128. [[CrossRef](#)]
39. Plaza-Garrido, M.; Salinas-Garcia, M.C.; Camara-Artigas, A. Orthorhombic Lysozyme Crystallization at Acidic PH Values Driven by Phosphate Binding. *Acta Cryst. D Struct. Biol.* **2018**, *74*, 480–489. [[CrossRef](#)]
40. Schirò, A.; Carlon, A.; Parigi, G.; Murshudov, G.; Calderone, V.; Ravera, E.; Luchinat, C. On the Complementarity of X-Ray and NMR Data. *J. Struct. Biol. X* **2020**, *4*, 100019. [[CrossRef](#)]

41. Torricella, F.; Pierro, A.; Mileo, E.; Belle, V.; Bonucci, A. Nitroxide Spin Labels and EPR Spectroscopy: A Powerful Association for Protein Dynamics Studies. *Biochim. Biophys. Acta Proteins Proteom.* **2021**, *1869*, 140653. [[CrossRef](#)]
42. Adiram-Filiba, N.; Ohaion, E.; Verner, G.; Schremer, A.; Nadav-Tsubery, M.; Lublin-Tennenbaum, T.; Keinan-Adamsky, K.; Lucci, M.; Luchinat, C.; Ravera, E.; et al. Structure and Dynamics Perturbations in Ubiquitin Adsorbed or Entrapped in Silica Materials Are Related to Disparate Surface Chemistries Resolved by Solid-State NMR Spectroscopy. *Biomacromolecules* **2021**, *22*, 3718–3730. [[CrossRef](#)]

**Disclaimer/Publisher's Note:** The statements, opinions and data contained in all publications are solely those of the individual author(s) and contributor(s) and not of MDPI and/or the editor(s). MDPI and/or the editor(s) disclaim responsibility for any injury to people or property resulting from any ideas, methods, instructions or products referred to in the content.